

## Comparison of Two-photon Optical Microscopies: Second-harmonic Generation and Fluorescence Imaging

Philip B. Lukins<sup>1,2</sup>, Pu Xu<sup>1</sup>, Shakil Rehman<sup>1</sup> and Colin J.R. Sheppard<sup>1</sup>

<sup>1</sup> Department of Physical Optics, School of Physics A28,

University of Sydney, NSW 2006, Australia

<sup>2</sup> National Measurement Laboratory,

CSIRO Division of Telecommunications and Industrial Physics,

Lindfield, NSW 2070, Australia

**Keywords:** two-photon microscopy, second-harmonic generation, two-photon excited fluorescence

**Abstract.** We describe the two-photon optical microscopy techniques of second-harmonic generation imaging and two-photon excited fluorescence imaging, and compare the principles, characteristics, imaging properties and performances of these techniques. We demonstrate these techniques for various specimens and imaging modes using a single femtosecond laser and a scanning microscope.

### Introduction

Confocal fluorescence laser scanning microscopy [1,2] has been widely used for three-dimensional (3D) high-resolution optical imaging of biological specimens. More recently, several nonlinear optical microscopies have been developed including those based on two-photon excited fluorescence [3,4], three-photon excited fluorescence [5], second-harmonic generation [6,7] and third-harmonic generation [8-10]. These nonlinear microscopies have also been shown to be valuable techniques for biomedical imaging [11-14] and their use is likely to become more widespread. These microscopies are based on the interaction between the high peak power density that exists at the laser focus and the nonlinear optical properties of the specimen in the focus region. The spatial variation of this interaction in the focus region gives a “soft-aperture” effect which leads to an inherent optical sectioning capability without the need for a confocal pinhole. The interest in these techniques stems partly from the greater penetration and hence imaging depth possible with the longer (usually near-infrared) wavelengths used, the reasonably high interaction efficiency especially for two-photon excited fluorescence, and the improved optical detection efficiency arising from the fact that a confocal pinhole is not required. While two-photon excited fluorescence (TPF) and second-harmonic generation (SHG) microscopies have been demonstrated using CW [6,15] and long-pulse [16] lasers, femtosecond sources are more desirable because the effect due to a given pulse varies inversely with the square of the laser pulsewidth for pulsed excitation.

TPF imaging is now a well-established technique with well-recognised applications, particularly in biology. On the other hand, SHG imaging is a technique that has found applications only relatively recently. This is partly due to the common availability nowadays of femtosecond lasers which maximise the SHG signal and the recent optimisation of SHG imaging [17]. SHG can be used as a probe of local anisotropy, the distribution of molecular hyperpolarisabilities, phase-matching properties, and surface plasmon enhanced interactions. Detectable second-harmonic light has been observed for a wide range of specimens including polycrystalline molecular films [18], thin films [16,19], aluminium [17,20] and gold [21] surfaces, and DNA and chromosomes [22]. High-resolution 3D SHG imaging using femtosecond laser pulses was demonstrated using LBO-based crystalline specimens [7]. SHG imaging has been used to probe membrane potentials [14,23-26] and image biological tissues [13,22, 27-32]. The significant SHG seen in biological materials arises from the low local symmetry and the large nonlinear coefficients typical of biological

molecules and structures. The main drawbacks of SHG imaging for biological or medical applications are that (a) the second-harmonic coefficients are small and the input intensity must be large in order to generate detectable signal, (b) the SHG signal normally propagates in the forward direction which may be inconvenient, and (c) a complete interpretation of the contrast-generating features in SHG imaging is difficult because of the various local second-order properties of the specimen, its molecular structure, the orientation of its microstructure with respect to both the direction and the polarization of the laser beam, and its possible absorption of both the excitation and second-harmonic light.

### Two-photon imaging

TPF is a 4-level resonant process involving effectively simultaneous absorption of two low energy photons of wavelengths  $\lambda_1$  and  $\lambda_2$  via a virtual state to cause electronic excitation to a real excited molecular vibronic state followed by fluorescent emission. This emission will have an angular distribution determined by the molecular configuration and a fluorescence decay time determined by the electronic upper-state lifetime (Fig. 1a). Relaxation back to the ground state occurs with emission of up-converted fluorescence where the wavelength of the fluorescence is slightly longer than  $1/(1/\lambda_1 + 1/\lambda_2)$ . In most cases, a single source is used so that  $\lambda_1 = \lambda_2 = \lambda$  and the emitted photon has a wavelength slightly greater than  $\lambda/2$ . For centrosymmetric or randomly-oriented fluorophores, the emission is isotropic. For other fluorophores, there will be an angular distribution of the fluorescence which reflects dipole, symmetry, and orientational effects. The fluorescence decay time is in the order of picoseconds or longer. Hence, fluorescence is incoherent.

On the other hand, SHG is of primarily electronic origin and is a non-resonant process. In SHG, two photons of the same wavelength “coalesce” to a virtual state within the specimen to form a single photon of energy exactly twice that of the incident photons (Fig. 1b). SHG is therefore a 3-level process. The second-harmonic photon is generated almost instantaneously (within a few fs) so that the second-harmonic signal is coherent.

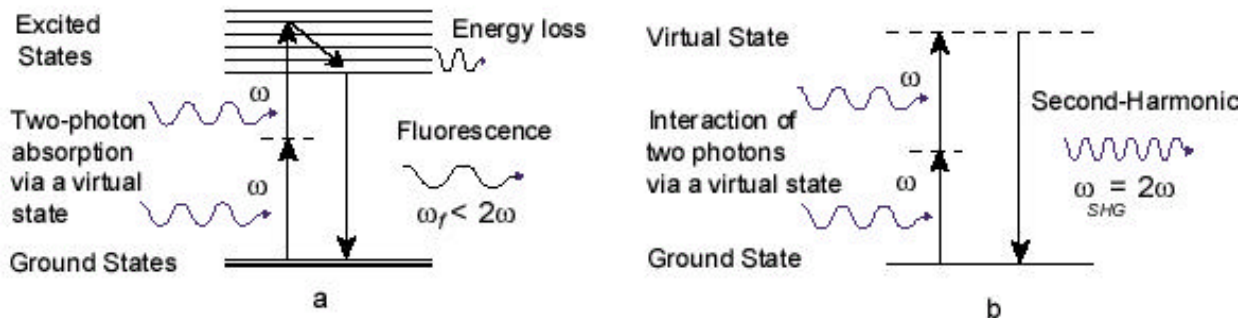


Fig. 1. Energy level diagram of TPF (a) and SHG (b) processes.

**Theoretical aspects.** The technique of TPF is now well-known. Unlike one-photon excited fluorescence where the fluorescence and input signals are linearly related, TPF exhibits a second-order dependence of fluorescence on instantaneous excitation power [4]. The TPF power  $P_{\text{TPF}}$  is related to the input power  $P_\omega$  by

$$P_{\text{TPF}} = \frac{1}{2} \sigma_A F P_\omega^2 \quad (1)$$

where  $\sigma_A$  is the two-photon absorption cross-section and  $F$  is the fluorescence quantum yield.

The theory of SHG and nonlinear optics [33] is well-known. The nonlinear terms contribute to the polarization only when the high-order terms of the Taylor expansion of  $E$  are non-negligible which is the case for a focused laser beam. Using a plane wave approximation, the second-harmonic power  $P_{2\omega}$  generated in a specimen which is illuminated by a fundamental laser beam of frequency  $\omega$ , wave vector  $k$ , and with input power  $P_{\omega}$ , can be expressed as

$$P_{2\omega} = c_2 \cdot \frac{P_{\omega}^2}{A} \cdot L^2 \cdot \frac{32\mathbf{p}^3\omega^3}{c^3\mathbf{e}(\omega)\sqrt{\mathbf{e}(2\omega)}} \left( \frac{\sin \Delta kL/2}{\Delta kL/2} \right)^2 \quad (2)$$

where  $A$  is the area of the focused spot,  $L$  is the length over which the fundamental laser beam interacts usefully with the material (the length of interaction),  $\epsilon(\omega)$  is the dielectric constant of the material,  $\omega = 2\pi/\lambda$ , and  $\Delta k = k_{2\omega} - 2k_{\omega}$ . The second-harmonic power is proportional to the square of the instantaneous peak power of the input. The elements of the tensor  $\chi_2$  reflect the symmetry and nonlinear optical properties of the material. Due to symmetry selection rules, it is found that the elements of  $\chi_2$  vanish for material with inversion symmetry. Hence, no SHG effect will be observed for an isotropic material or for centrosymmetric molecules. Together with this restriction, the specimen must be relatively transparent to the fundamental illumination wavelength and the generated harmonics. For a phase-matched uniform crystal, the harmonic radiation is generated in the forward direction [33]. However, for more complex materials, such as biological membranes, the SHG signal has a marked two-lobe angular distribution which arises from both phase and polarisation effects [29]. In two-photon microscopy, the excitation probability is proportional to the square of the fundamental incident intensity. Hence, the spatial properties of two-photon interactions provide a useful mechanism for optical sectioning in such microscopes via a ‘‘soft-aperture’’ effect. Because there is little signal from regions away from the point of focus, out-of-focus interference is virtually eliminated. In this case, the optical sectioning arises from the illumination system in contrast to confocal operation where the optical sectioning arises from spatially filtering the photons using a small aperture. Therefore, the effective spot size produced in the specimen is sharpened by a factor of  $\sqrt{2}$ . This can be understood by the fact that if the fundamental intensity profile has a Gaussian distribution, then the signal intensity profile will also have a Gaussian distribution, but with an effective radius of  $1/\sqrt{2}$  of that of the fundamental. Hence, the size of the effective point spread function is reduced by a factor of  $\sqrt{2}$  and a form of super-resolution is obtained. Accordingly, the Rayleigh criterion can be expressed as

$$x_{\min} = 0.43 \lambda / \text{NA} \quad (3)$$

where  $x_{\min}$  is the minimum resolvable distance,  $\lambda$  is the illumination wavelength and NA is the numerical aperture of the microscope objective. In order to optimize the resolution in SHG and make  $x_{\min}$  as small as possible, one can either decrease the illumination wavelength or increase the numerical aperture. Since the illumination wavelength in SHG imaging is not specimen-dependent (apart from specimen absorption properties) one could use the shortest wavelength available from a pulsed laser or the frequency-converted output of such a laser. In contrast, fluorescence imaging requires that the illumination wavelength be chosen according to both the absorption and fluorescence properties of the specimen.

**Instrumental realization.** A layout of a generalised two-photon microscope is shown in Fig. 2. Basically, it incorporates a laser (usually a femtosecond laser) and a 3D scanning optical microscope [22]. We used a modified inverted Leica TCS NT beam-scanning confocal microscope coupled to a Coherent Mira 900 femtosecond Ti:sapphire laser. For these laser pulsewidths ( $\sim 100$

fs), an adjustable group velocity dispersion precompensation arrangement was not necessary [34]. The laser beam is focused into the specimen with a high NA microscope objective (x40 0.75NA). The second-harmonic signal is collected with a lens in transmission mode (or using a dichroic in reflection mode) and the fluorescence signal is detected in reflection. An important capability of this system is that it can operate simultaneously in both transmission and reflection modes. For the fluorescence channel, a broadband dichroic was used and the fluorescence detection bandwidth determined by a long-pass filter with a cutoff wavelength  $\sim 450$  nm. For the SHG channel, the 800 nm fundamental beam was excluded from the detector using a 400 nm interference filter with a FWHM of 20 nm. Although SHG detection in the forward direction is more efficient, operation in reflection is also possible provided that the second-harmonic light is back-scattered by the specimen or retro-reflected by means of a mirror substrate. It should be noted that the frequency bandwidth of the detector and amplifier must be greater than the pixel scan rate but smaller than the repetition rate of the laser. The observed resolution for both TPF and SHG modes was  $\sim 0.5$   $\mu\text{m}$  which is close to the theoretical value of  $0.46$   $\mu\text{m}$  from Eq. 3. The resolution can be maximised by using a confocal pinhole while the collection efficiency is maximised when no aperture is used.

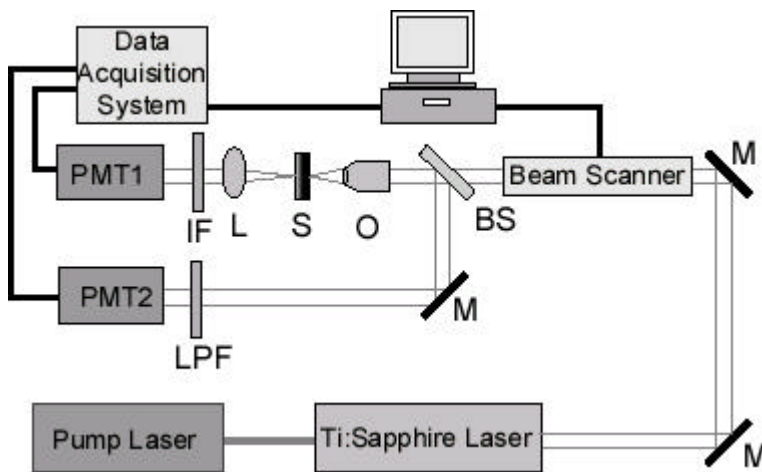


Fig. 2. Experimental arrangement of SHG/TPF microscope. For SHG imaging, optical filtering is achieved with an interference filter centered on the second harmonic frequency whereas for TPF imaging, a long-pass filter is selected with a cut-off frequency according to the fluorescence emission spectrum. BS, beamsplitter; IF, 400 nm interference filter; L, lens; LPF, long-pass filter; M, mirror; O, objective; S, specimen.

**Performance and optimization.** Several experimental factors influence the performance of two-photon microscopes. These include the pulse width, average power, peak power and wavelength of the laser, the polarization of the incident laser beam or the detected light, the magnification and numerical aperture of the microscope objective, the length of interaction, the detection geometry of the imaging system, and inter-dependences between these factors.

As seen from Eq. (1) and (2), as well as numerous experimental studies, the TPF and SHG powers are proportional to the square of the instantaneous power  $P_\omega$  of the fundamental beam. Furthermore, the signal increases as the pulsewidth decreases. Hence, the average TPF or SHG signal  $\langle P \rangle$  varies with the average fundamental power  $\langle P_\omega \rangle$  and the laser pulsewidth  $\tau$  [17]:

$$\langle P \rangle \sim \langle P_\omega \rangle / \tau \quad (4)$$

In TPF imaging, the specimen should be relatively transparent at both the fundamental and fluorescent wavelengths but somewhat absorbing at half the illumination wavelength so that two-photon absorption can occur. In SHG imaging, on the other hand, the specimen should be relatively transparent at both the fundamental and harmonic wavelengths. In either imaging method, it is therefore the shape of the absorption spectrum of the specimen that determines the usable wavelengths for illumination and detection. The resolutions for the two methods will be very similar for largely transparent specimens. For most real specimens, particularly biological ones, both TPF (due to autofluorescence) and SHG will occur at the same time. The efficiency of TPF processes will decrease when the wavelength spectrum of the excitation, which broadens with the shortening of pulses, is wider than the absorption spectrum of the fluorophore. For SHG imaging,

the process is non-absorbant and so pulses as short as possible are desirable. Although autofluorescence can be observed in TPF imaging, in order to increase the contrast of their most interesting features, specimens are generally labelled with dyes or fluorescent probes. Contrast in SHG imaging is guaranteed since the second-harmonic coefficients vary between and within regions in a specimen and between different molecular systems which may occur within a given specimen. Apart from laser-induced dielectric breakdown and thermal damage, the technique is non-invasive. It should be noted that whereas in TPF imaging there is a lower bound on the optimal length of the excitation pulse width, this is not the case for SHG imaging provided pulse broadening due to dispersion effects from the optics in the microscope can be adequately compensated.

Polarisation of the incident laser beam is a crucial factor in two-photon imaging but has received relatively little attention so far. However, Higdon et al. [35] have developed a theory for TPF imaging under high NA conditions and Moreaux et al. [29,30] have developed an analogous theory for SHG imaging. Stoller et al. [31] have extended these studies by performing polarisation studies and implementing a novel polarisation modulation technique to enable polarisation mapping of the SHG signal generated by collagen, muscle and other fibrous biological materials.

High-resolution nonlinear imaging normally requires objectives with magnifications of at least x40. At low NA the narrower angular distribution of the focused beam can provide a better match to the axes of the molecular dipole or second-order nonlinearity than is the case for high NA imaging where the angular distribution is much broader and so a smaller fraction of the incident light is oriented in the appropriate direction. When the NA is increased, the focus spot size will be tighter resulting in higher resolution but will lead to a decrease in interaction length and signal level. The contrast in the image may also decrease with increasing NA since the angular spectrum will be greater. Therefore, the effect of the NA is not obvious because it depends on sample structure. Nevertheless, for high NA microscope objectives, phase-matching is not important and SHG images arise purely from a local molecular nonlinear effect. Furthermore, when SHG images are collected in reflection, reducing the NA also plays a role in the collection efficiency of the second-harmonic light. From the above discussion, it is clear that a general theory for two-photon imaging under high NA illumination conditions is required [35].

For a microscope objective which produces an ideal focus, the phase-coherent interaction length  $L$  is given by [36]

$$L = \frac{2\mathbf{p}c}{\mathbf{w}n_1} \left[ \frac{n_2}{n_1} - \cos\mathbf{q} \right]^{-1} \quad (5)$$

where  $n_1$  and  $n_2$  are the refractive indices for the fundamental and second-harmonic waves in the specimen, and  $\theta$  is the angular direction of propagation. Although phase-matching and signal level can be optimised by increasing  $L$ , this is not desirable for high resolution SHG imaging where  $L$  must necessarily remain as small as possible.

Although a non-confocal detection method is usually used for both TPF and SHG imaging in order to maximise sensitivity, improved resolution can be obtained by using a confocal pinhole albeit at the expense of signal level [37,38]. An example of a simple layout for multichannel two-photon microscopy with enhanced spatial resolution might consist of two independent fluorescence detection channels (with and without pinholes) in either a reflection configuration, as used here, or in a transmission mode using dichroics to separate the fluorescence signals from harmonic signals which are best detected in transmission in this case. Differential processing of the separate images from the multiple detectors should also yield a useful resolution enhancement.

**Relative sensitivity and signal levels.** Similarly to fluorescence imaging, SHG can be enhanced by a number of labelling methods such as the use of gold nanoparticles or gold-labelled antibodies [25] and staining with styryl dyes [14]. Another method to increase the SHG signal is to exploit surface plasmon interactions which can lead to an enhancement of the SHG by a factor of up to  $10^4$  for

particular surfaces [17]. The enhancement depends on the extent of the surface roughness and the mechanism of interaction between the roughness and the surface plasmons. Surface plasmon enhanced SHG can be separated from other surface phenomena such as surface enhanced Raman scattering by examining the spectrum of the emitted light.

When comparing TPF and SHG imaging, it is of interest to consider the relative magnitudes of the respective signal levels. A quantitative comparison is very difficult because there are many experimental and specimen factors that are important, perhaps the most important ones being that TPF and SHG are probing different specimen properties and that there are wide variations of as much as several orders of magnitude in the signal levels both within and between specimens. Nevertheless, indicative ranges for the conversion efficiencies and laser power levels used for both TPF and SHG microscopy are (0 - 30 %, < 20 mW) and (0 - 20 %, < 50 mW) respectively. As a rough guide, for most biological specimens the SHG signal is typically smaller than, but within an order of magnitude of, the TPF signal arising from autofluorescence. For the results presented here, the typical range of maximum average powers produced was 1 nW – 10  $\mu$ W for SHG imaging and 5 nW – 50  $\mu$ W for TPF imaging.

**Applications of TPF and SHG imaging.** TPF and SHG imaging have now been widely applied as separate imaging techniques. However, a multichannel imaging approach may be particularly attractive because the laser pulse may interact with several nonlinear optical properties of the specimen and the resulting optical signals may be detected separately to form composite nonlinear optical images of the specimen. This approach can be taken by either separately applying TPF and SHG imaging in turn to a given specimen or by acquiring TPF and SHG images simultaneously in time on a given specimen. Peleg et al. [25] have adopted the former approach to image neurons. More recently, Gauderon et al. [22] have demonstrated two-channel TPF/SHG imaging of chromosomes with simultaneous image acquisition and Moreaux et al. [29,30] have reported simultaneous TPF/SHG imaging of vesicles and cellular structures.

The literature now contains numerous reports of imaging using TPF or SHG, but very few where the two techniques are compared directly or even used simultaneously. The spectrum (Fig. 3a) of light generated by illumination of a ZnO ceramic specimen with 890 nm pulses reveals a SHG peak at 445 nm and a broad fluorescence/luminescence band from 450 – 700 nm. Therefore, imaging using light selectively collected at 445 nm and 450 – 700 nm enables SHG and TPF imaging respectively (Fig. 3b,c). We have used this approach to obtain 2D and 3D SHG and TPF images of a wide range of specimens in both the separate and simultaneous modes. In Fig. 4, we demonstrate simultaneous TPF/SHG imaging for various specimens ranging from biomolecular to protein to cellular systems. TPF imaging provides excellent sensitivity and contrast for a wide range of structures and is particularly useful for cellular imaging. SHG imaging provides less overall sensitivity for a range of structures but yields enhanced contrast and structural specificity for certain highly-oriented structures. For example, in the rat tissue images (Fig. 4e,f) TPF images the whole structure effectively whereas SHG is much less sensitive to the cellular features but detects the collagen-based structural matrix with extremely high sensitivity. The complementary use of both methods allows one to distinguish the cellular and matrix components of the tissue with stunning clarity. Compared with TPF imaging, SHG imaging typically gives images that are more binary in appearance, that is, they show extremely high contrast or signal in regions of high nonlinearity but extremely low contrast or signal in regions of low nonlinearity. This effect is seen in all the SHG images in Fig. 4. There are features that appear common to each image and others that are clearly unique to one image or the other. Simultaneous acquisition of TPF and SHG images clearly provides an excellent means of obtaining new and complementary information. Simultaneous imaging would also be very useful for time-series studies, in cases where photodamage must be minimised and where specimen changes or drift occur during the scan period.

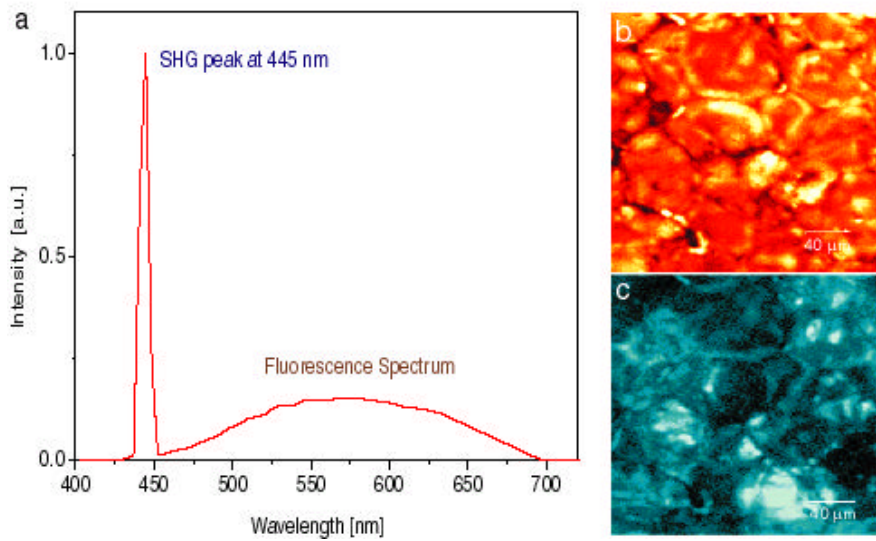


Fig. 3. Spectrum of light collected from a ZnO ceramic specimen excited at 890 nm with 110 fs pulses (a) together with the TPF (b) and SHG (c) images obtained near the ceramic surface.

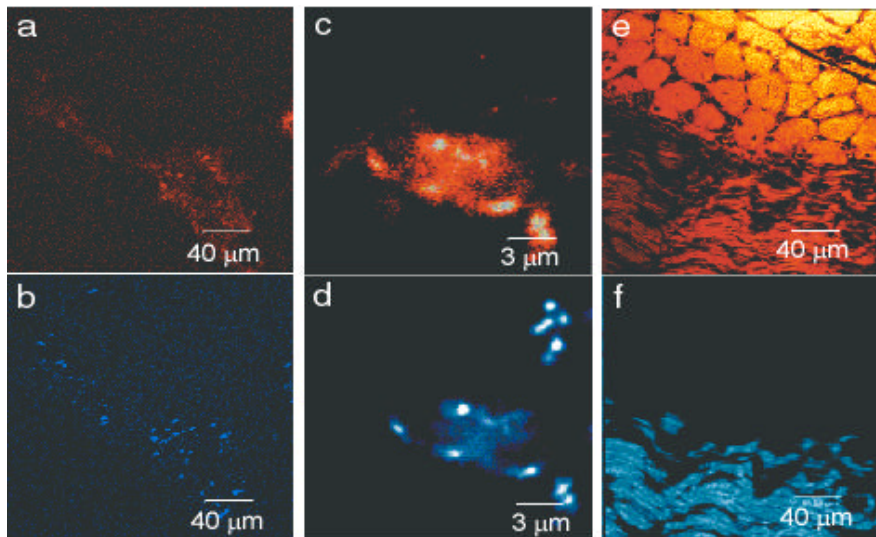


Fig. 4. Comparison of TPF and SHG images of various biological specimens. For each specimen, the upper images (a, c, e) are TPF images and the lower images (b, d, f) are SHG images. The (unstained) specimens are DNA fragments (a, b), fruit fly chromosomes (c, d) and rat-tail tendon (e, f).

## Conclusions

We have demonstrated TPF and SHG imaging and shown that these techniques can be implemented using available lasers and confocal microscopes together with only a few additional components. The combined or simultaneous use of two or more multiphoton microscopic techniques, such as TPF and SHG imaging, will become increasingly important in 3D biomedical applications. A variety of multichannel multiphoton microscopies can be implemented using flexible and reconfigurable laser/microscope systems in combination with exploitation of two or more multiphoton interactions and different detector configurations.

## References

- [1] J.B. Pawley: *Handbook of Biological Confocal Microscopy* (Plenum Press, London 1985).
- [2] S.W. Paddock: *Confocal Fluorescence Microscopy: Methods and Protocols* (Humana Press, New Jersey 1999).
- [3] C.J.R. Sheppard and R. Kompfner: *Appl. Opt.* **17**, 2879-2882 (1978).
- [4] W. Denk, J. Strickler and W. Webb: *Science* **248**, 73-76 (1990).
- [5] S.W. Hell, K. Bahlmann, M. Schrader, M. Soini, H. Malak, I. Gryczynski and J. Lakowicz: *J. Biomed. Opt.* **1**, 71-74 (1996).

- [6] J. Gannaway and C.J.R. Sheppard: *Opt. Quant. Electron.* **10**, 435-439 (1978).
- [7] R. Gauderon, P.B. Lukins and C.J.R. Sheppard: *Opt. Lett.* **23**, 1209-1212 (1998).
- [8] Y. Barad, H. Eisenberg, M. Horowitz and Y. Silberberg: *Appl. Phys. Lett.* **70**, 922-924 (1996).
- [9] M. Muller, J. Squier, K.R. Wilson and G.J. Brakenhoff: *J. Microsc.* **191**, 266-274 (1998).
- [10] J.A. Squier, M. Mueller, G.J. Brakenhoff and K.R. Wilson: *Opt. Exp.* **3**, 315-324 (1998).
- [11] W. Denk: *J. Biomed. Opt.* **1**, 296-304 (1996).
- [12] K. Konig: *J. Microsc.* **200**, 83-104 (2000).
- [13] Y. Guo, P.P. Ho, H. Savage, D. Harris, P. Sacks, S. Schantz, F. Liu, N. Zhadin and R.R. Alfano: *Opt. Lett.* **22**, 1323-1325 (1997).
- [14] P.J. Campagnola, M. Wei, A. Lewis and L.M. Loew: *Biophys. J.* **77**, 3341-3349 (1999).
- [15] M.J. Booth and S.W. Hell: *J. Microsc.* **190**, 298-304 (1998).
- [16] J. Vydra and M. Eich: *Appl. Phys. Lett.* **72**, 275-277 (1998).
- [17] R. Gauderon, P.B. Lukins and C.J.R. Sheppard: *Micron* **32**, 691-700 (2001).
- [18] T. Jentsch, H.J. Jupner, S.H. Ashworth and T. Elsaesser: *Opt. Lett.* **21**, 492-494 (1996).
- [19] D.J. Bottomley, A. Mito, S. Niki and A. Yamada: *Opt. Lett.* **21**, 254-257 (1996).
- [20] S. Janz, K. Pedersen and H.M van Driel: *Phys. Rev. B* **44**, 3943-3946 (1991).
- [21] S.D. Moustazis, N.A. Papadogiannis, C. Fotakis, G. Farkas and C. Toth: *Appl. Phys. Lett.* **67**, 3239-3242 (1995).
- [22] R. Gauderon, P.B. Lukins and C.J.R. Sheppard: *Micron* **32**, 685-689 (2001).
- [23] O. Bouevitch, A. Lewis, I. Pinevsky, J.P. Wuskell and L.M. Loew: *Biophys. J.* **65**, 672-679 (1993).
- [24] A. Lewis, A. Khatchaturiants, M. Treinin, Z. Chen, G. Peleg, N. Friedman, O. Bouevitch, Z. Rothman, L. Loew and M. Sheres: *Chem. Phys.* **245**, 133-144 (1999).
- [25] G. Peleg, A. Lewis, M. Linial and L.M. Loew: *Proc. Natl. Acad. Sci. USA* **96**, 6700-6704 (1999).
- [26] L. Marrucci, D. Paparo, G. Cerrone, C. de Lisio, E. Santamato, S. Solimeno, S. Ardizzone and P. Quagliotto: *Opt. Lasers Eng.* **37**, 601-610 (2002).
- [27] I. Freund, M. Deutsch and A. Sprecher: *Biophys. J.* **50**, 693-712 (1986).
- [28] Y. Guo, P.P. Ho, A. Tirkslunas, F. Liu and R.R. Alfano: *Appl. Opt.* **35**, 6810-6813 (1996).
- [29] L. Moreaux, O. Sandre and J. Mertz: *J. Opt. Soc. Am. B* **17**, 1685-1694 (2000).
- [30] L. Moreaux, O. Sandre, S. Charpak, M. Blanchard-Desce and J. Mertz: *Biophys. J.* **80**, 1568-1574 (2001).
- [31] P. Stoller, K.M. Reiser, P.M. Celliers and A. Rubenchik: *Biophys. J.* **82**, 3330-3342 (2002).
- [32] P.J. Campagnola, A.C. Millard, M. Terasaki, P.E. Hoppe, C.J. Malone and W.A. Mohler: *Biophys. J.* **81**, 493-508 (2002).
- [33] N. Bloembergen: *Nonlinear Optics* (World Scientific, New York 1965).
- [34] R.L. Fork, O.E. Martinez and J.P. Gordon: *Opt. Lett.* **9**, 150-152 (1984).
- [35] P.D. Higdon, P. Torok and T. Wilson: *J. Microsc.* **193**, 127-141 (1999).
- [36] G.D. Boyd and D.A. Kleinman: *J. Appl. Phys.* **39**, 3597-3639 (1968).
- [37] E.H.K. Stelzer, S. Hell, S. Lindek, R. Stricker, R. Pick, C. Storz, G. Ritter and N. Salmon: *Opt. Commun.* **104**, 223-228 (1994).
- [38] R. Gauderon, P.B. Lukins and C.J.R. Sheppard: *Microsc. Res. & Tech.* **47**, 210-214 (1999).